# Coupled Modes of the Warm Pool Climate System. Part I: The Role of Air–Sea Interaction in Maintaining Madden–Julian Oscillation

BIN WANG AND XIAOSU XIE*

*Department of Meteorology, University of Hawaii, Honolulu, Hawaii*

(Manuscript received 7 April 1997, in final form 3 September 1997)

ABSTRACT

Over the warm pool of the equatorial Indian and western Pacific Oceans, both the climatological mean state and the processes of atmosphere–ocean interaction differ fundamentally from their counterparts over the cold tongue of the equatorial eastern Pacific. A model suitable for studying the coupled instability in both the warm pool and cold tongue regimes is advanced. The model emphasizes ocean mixed layer physics and thermodynamical coupling that are essential for the warm pool regime. Different coupled unstable modes are found under each regime.

In contrast to the cold tongue basic state, which favors coupled unstable low-frequency SST mode, the warm pool regime (moderate mean surface westerlies and deep thermocline) is conducive for high-frequency (intraseasonal timescale) coupled unstable modes. The wind–mixed layer interaction through entrainment/evaporation plays a central role in the warm pool instability. The cloud-radiation feedback enhances the instability, whereas the ocean wave dynamics have little impact. The thermodynamic coupling between the atmosphere and ocean mixed layer results in a positive SST anomaly leading convection, which provides eddy available potential energy for growing coupled mode. The relatively slow mixed layer response to atmospheric forcing favors the growth of planetary-scale coupled modes. The presence of mean westerlies suppresses the low-frequency SST mode.

The characteristics of the eastward-propagating coupled mode of the warm pool system compares favorably with the large-scale features of the observed Madden–Julian Oscillation (MJO). This suggests that, in addition to atmospheric internal dynamic instability, the ocean mixed layer thermodynamic processes interacting with the atmosphere may play an active part in sustaining the MJO by (a) destabilizing atmospheric moist Kelvin waves, (b) providing a longwave selection mechanism, and (c) slowing down phase propagation and setting up the 40–50-day timescale.

## 1. Introduction

The development of El Niño–Southern Oscillation (ENSO) is generally understood as resulting from coupled instability of the tropical ocean–atmosphere system (e.g., Philander et al. 1984; Yamagata 1985; Hirst 1986; Neelin 1991). In the ocean models used for the coupled instability analysis, the sea surface temperature (SST) variations are controlled by dynamic processes associated with thermocline displacement and temperature advection by currents and upwelling. These dynamic processes are indeed of central importance for the coupled instability of the eastern Pacific and for sustaining basinwide ENSO cycle (e.g., Cane and Zebiak 1985; Suarez and Schopf 1988; Battisti and Hirst 1989). However, the ocean wave dynamics are not critical to SST changes in the warm pool (SST is normally higher than 28°C) of the tropical western Pacific and Indian Oceans where thermocline is deep and horizontal SST gradients are small.

The interaction of atmosphere and ocean over the warm pool occurs on a broad range of timescales ranging from intraseasonal to interannual or even longer. The interaction on the intraseasonal timescale appears to be at least as vigorous as that on the ENSO timescale. Prior to the Tropical Ocean Global Atmosphere Coupled Ocean–Atmosphere Response Experiment (TOGA COARE), Krishnamurti et al. (1988) estimated that the magnitude of SST variations on the 30–50-day timescale was about 0.5°–1.0°C. Recent TOGA COARE observations reveal prominent intraseasonal variability in both the SST and mixed layer depth. The amplitude of SST variation associated with the Madden–Julian Oscillation (MJO) (Madden and Julian 1971) exceeds 1.0°C (Lau and Sui 1997). This intraseasonal variability is larger than that on the annual and ENSO timescales.

The warm pool air–sea interaction involves processes

*Current affiliation: Jet Propulsion Laboratory, California Institute of Technology, Pasadena, California.

*Corresponding author address:* Dr. Bin Wang, Department of Meteorology, University of Hawaii, 2525 Correa Rd., Honolulu, HI 96822.
E-mail: bwang@soest.hawaii.edu

that differ from those over the cold tongue region. The coupling between cloud–wind and ocean mixed layer thermodynamic processes is of central importance. TOGA COARE analyses indicate that the variability in precipitation and cloud is, to a large extent, controlled by the MJO (Johnson 1995). Thus, the MJO can regulate shortwave radiative heating in the ocean mixed layer via changing cloudiness. Strong turbulent mixing and entrainment as well as latent heat loss associated with westerly wind bursts during the wet phase of MJO may also cause considerable cooling of the mixed layer. This results in a spatial phase relationship between SST and atmospheric circulation: positive SST anomalies lead convective anomalies by about a quarter of period (e.g., Kawamura 1988; Nakazawa 1995; Zhang 1996). On the other hand, atmospheric thermodynamic variables, such as precipitable water vapor and convective available potential energy, tend to follow SST variation and lead convection anomalies (Chou et al. 1995; Fasullo and Webster 1995). Significant variation of SST on intraseasonal timescales has the potential to impact on atmospheric MJO, but the degree to which and the way by which SST affects the MJO are not known.

Whereas the warm pool system involves active ocean–atmosphere interaction on both intraseasonal and ENSO development timescales, the nature of the coupled mode has not been explored with an adequate theoretical model. The majority of coupled-instability models treat the atmosphere as a ''slave'' and thus exclude high-frequency coupled modes. Lau and Shen (1988) and Hirst and Lau (1990) realized this problem. They took into account the transient atmospheric waves in their atmospheric models. However, the ocean–atmosphere coupling in their models is essentially the same dynamic coupling that is suitable for the cold tongue regime; the processes that are important for SST variation in the warm pool, such as wind- and cloud-induced anomalous diabatic heating, are absent. It is, therefore, necessary to investigate the coupled modes that may result from the distinctive cloud–wind–mixed layer thermodynamic coupling processes prevailing in the warm pool.

Specific questions to be addressed include the following. What is the nature of the coupled ocean–atmosphere modes under warm pool basic state and prevailing thermodynamic coupling processes? How does the ocean–atmosphere interaction contribute to the stability of the coupled warm pool system? To what degree, and how, does the ocean feed back to the MJO?

The main purpose of the present study is to investigate the impacts of oceanic mixed layer processes and ocean–atmosphere thermodynamic coupling on coupled instability. In the next section, a new theoretical model is formulated for coupled stability analysis in the warm pool regime. In section 3 a family of progressively reduced physics models are used to identify roles of different coupling processes in stimulating coupled instability. Section 4 further examines the dynamic structure and energy conversion of the coupled unstable modes to understand why the warm pool mean state and the thermodynamical coupling favor development of coupled high-frequency modes. In section 5, the coupled instability of the cold tongue regime is briefly discussed in order to contrast the warm pool instability. Section 6 compares TOGA COARE observations with the theory and articulates the potential roles of the ocean mixed layer interacting with the atmosphere in sustaining MJO. The last section summarizes key points and discusses the limitations of the warm pool instability theory.

## 2. The coupled atmosphere–ocean model for the warm pool climate system

### *a. The model equations*

The atmospheric model describes linear motion of the lowest baroclinic mode, which is stimulated by condensational heating (Gill 1980). The heating rate is assumed to be proportional to anomalous SST. This elementary form was derived from different perspectives in the past by considering various processes such as convective parameterization (Philander et al. 1984; Hirst 1986), evaporation (Zebiak 1986), longwave Newtonian relaxation (Davey and Gill 1987), or equivalent SST gradient effect (Lindzen and Nigam 1987; Neelin 1989). The governing equations in p coordinates for the gravest baroclinic mode on an equatorial $\beta$ plane are

$$\frac{\partial U}{\partial t} + \varepsilon_a U - \beta y V = -\frac{\partial \phi}{\partial x}, \tag{2.1a}$$

$$\frac{\partial V}{\partial t} + \varepsilon_a V + \beta y U = -\frac{\partial \phi}{\partial y}, \quad \text{and} \tag{2.1b}$$

$$\frac{\partial \phi}{\partial t} + \mu_a \phi + C_a^2(1 - I)\left(\frac{\partial U}{\partial x} + \frac{\partial V}{\partial y}\right) = -\frac{Rg}{2C_p p_2}\alpha_a T, \tag{2.1c}$$

where $U$, $V$, and $\phi$ are lower-tropospheric zonal and meridional wind and geopotential, respectively; $\varepsilon_a$ and $\mu_a$ are, respectively, coefficients for Rayleigh friction and Newtonian cooling; $C_a$ is a dry atmospheric Kelvin wave speed; $I$ denotes a heating coefficient associated with wave-induced moisture convergence, which is a function of mean SST (Wang 1988a), thus the moist Kelvin wave speed $C_a^* = C_a(1 - I)^{1/2}$; $\alpha_a$ is a latent heating coefficient; $T$ is SST or ocean mixed layer temperature anomaly; and $R$, $g$, $C_p$, and $p_2$ denote the gas constant, gravity, specific heat at constant pressure, and the pressure at the middle troposphere, respectively. Equations (2.1a)–(2.1c) are essentially the same as the atmospheric model used by Hirst and Lau (1990), except a heating term related to the zonal wind anomaly was neglected. The effect of the neglected term on the coupled instability was discussed in detail by Hirst and Lau (1990).

The ocean model differs from those used in previous coupled stability analyses. The atmosphere and ocean

interact through both momentum and heat exchanges at the ocean surface. The heat exchange is influenced by cloudiness via changing shortwave radiational heating and by surface winds via changing turbulent entrainment and surface evaporation. Detailed derivation of the ocean model is given in the appendix.

Over the warm pool, the governing equations for the perturbation motion in the active upper ocean and the embedded mixed are (see appendix)

$$\frac{\partial u}{\partial t} - \beta y v = -b\frac{\partial h}{\partial x} + \alpha_o U - \varepsilon_o u, \tag{2.2a}$$

$$\frac{\partial v}{\partial t} - \beta y u = -b\frac{\partial h}{\partial y} + \alpha_o V - \varepsilon_o v, \tag{2.2b}$$

$$\frac{\partial h}{\partial t} + H\left(\frac{\partial u}{\partial x} + \frac{\partial v}{\partial y}\right) = 0, \tag{2.2c}$$

$$\frac{\partial h_1}{\partial t} = E\overline{U}U + \overline{w}_e\left(\frac{3U}{\overline{U}} + \frac{h}{H_2} - \frac{H}{H_2}\frac{h_1}{H_1}\right), \tag{2.2d}$$

and

$$\frac{\partial T}{\partial t} = D_{rad}\left(\frac{\partial U}{\partial x} + \frac{\partial V}{\partial y}\right) - D_{ent}\left(\frac{3U}{\overline{U}} - \frac{h_1}{H_1}\right) - D_{eva}\left(\frac{U}{\overline{U}} + \frac{T}{\overline{T} - 293}\right) - \mu_o T, \tag{2.2e}$$

where dependent variables are vertical mean upper-ocean zonal ($u$) and meridional ($v$) velocity, thermocline depth ($h$), mixed layer depth ($h_1$), and mixed layer temperature ($T$); $b$ is the buoyancy (reduced gravity); $\varepsilon_o$ is Rayleigh damping coefficients in the upper ocean; $H_1$ and $H$ denote the mean depths of the mixed layer and thermocline, respectively; $H_2 = H - H_1$; $\alpha_o$ is a wind stress coefficient; $E$ is Ekman pumping coefficient [Eq. (A1e′)]; $\overline{w}_e$ is the mean entrainment rate [Eq. (A3a)]; $\mu_o$ is a Newtonian cooling coefficient in the ocean mixed layer; and $D_{rad}$, $D_{ent}$, and $D_{eva}$ are, respectively, the mixed layer heating coefficients associated with shortwave radiation, entrainment, and evaporation processes. These coefficients are defined by Eqs. (A.6a)–(A.6d).

### b. Model physics and parameters

Figure 1 schematically summarizes the physics of the present coupled model. The mixed layer temperature affects atmospheric heating and changes lower-tropospheric geopotential and surface winds. Changes in surface winds alter mixed layer temperature through directly changing evaporation rate, entrainment rate, and surface convergence/cloudiness (thus the shortwave radiation flux). The surface winds also control thermocline displacement $h$ via generating oceanic waves/currents and influence mixed layer depth $h_1$ via Ekman pumping. Both the variations in $h$ and $h_1$ would further modify mixed layer temperature.

Typical values of the model parameters used in the present model are given in Table 1. The empirical coefficient $\lambda$ measures the proportionality between perturbation cloudiness and surface wind convergence. A value of $2 \times 10^5$ s means that an anomalous surface wind convergence of $5 \times 10^{-7}$ s$^{-1}$ may result in an increase in total cloudiness by one-tenth.

The characteristic parameters for the western and eastern Pacific mean states are listed in Table 2. Over the warm pool, it is assumed that mean surface frictional velocity $\overline{u}_* = 0.48$ cm s$^{-1}$ and the entrainment layer depth is 10 m. The corresponding mean entrainment rate $\overline{w}_e = 2 \times 10^{-6}$ m s$^{-1}$ [see Eq. (A.3a)], which induces a cooling rate that balances mean net downward heat flux $\overline{Q}_0 \doteq 15$ W m$^{-2}$ [see Eq. (A.3b)]. The estimated mean downward solar radiation flux for mean cloudiness $\overline{C} = 0.6$ is 190 W m$^{-2}$. The typical value $\alpha_a = 12$ kg s$^{-3}$ K$^{-1}$ and mean SST $\overline{T} = 303$ K yield a mean surface latent heat flux of about 120 W m$^{-2}$. The estimated mean longwave radiation flux with a coefficient $\gamma = 1.8$ W m$^{-2}$ K$^{-1}$ (Seager et al. 1988) is $-55$ W m$^{-2}$. These estimates approximately match TOGA COARE observations (Godfrey et al. 1995; Lau and Sui 1997).

There are a number of coupling coefficients whose values depend on the basic state (Table 2). The wind stress coefficient $\alpha_o = (\rho_a C_D|\overline{U}|/\rho_o H)$ determines the efficiency of the atmospheric momentum flux into the ocean, where $C_D$ is drag coefficient, $\rho_o = 10^3$ kg m$^{-3}$ the reference density in the deep ocean layer, $\rho_a = 1.2$ kg m$^{-3}$ the air density in the atmospheric boundary layer, and $\overline{U}$ the mean surface zonal wind. The latent heating coefficient $\alpha_a = \rho_a C_E L_C K_q|\overline{U}|$ determines the efficiency of latent heat flux into the atmosphere, where $L_c$ and $C_E$ represent latent heat and moisture exchange coefficients, respectively; $K_q = 8.9 \times 10^{-4}$ K$^{-1}$ (Wang and Li 1993). The coefficients $D_{rad}$, $D_{ent}$, and $D_{eva}$ [defined by (A.6a), (A.6b), and (A.6c)] measure, respectively, the degree of influence on SST from cloud-dependent radiation flux, wind-dependent entrainment, and evaporation.

### c. Numerical scheme

Normal mode solutions of Eqs. (2.1) and (2.2) are sought of the form:

$$(U, V, \phi, u, v, h, h_1, T) = \mathrm{Re}[U, \tilde{V}, \tilde{\Phi}, \tilde{u}, \tilde{v}, \tilde{h}, \tilde{h}_1, \tilde{T}]e^{i(kx-\sigma t)}, \tag{2.3a}$$

where "~" denotes corresponding meridional structure, $k$ is nondimensional wavenumber, and $\sigma$ is frequency (eigenvalue). The lateral boundary conditions are

$$(U, V, \phi, u, v, h, h_1, T) = 0 \quad \text{at} \quad y = \pm Y_b. \tag{2.3b}$$

With application of (2.3a,b), a finite-difference scheme in the meridional direction transforms Eqs. (2.1) and (2.2) into a linear algebraic system, which was solved by matrix inversion. As the meridional boundary

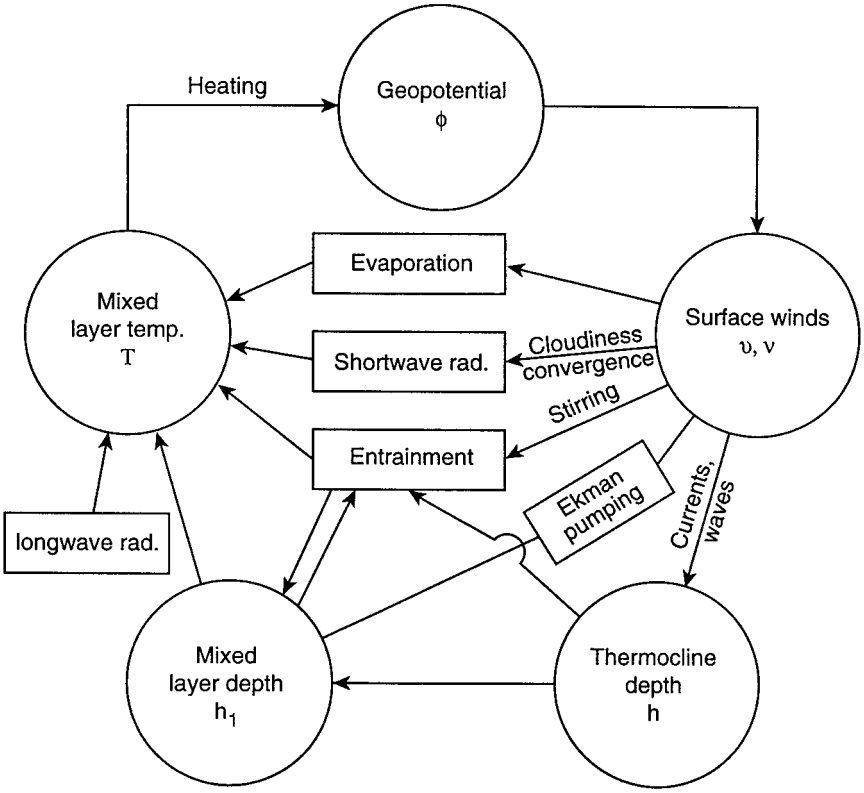


FIG. 1. Schematic diagram highlighting the model physics.

($Y_b$) was set beyond 20° and the resolution ($\Delta y$) less than 0.75°, the solutions of the principal unstable modes were not sensitive to the changes in $Y_b$ and $\Delta y$, indicating that $Y_b = 20°$ and $\Delta y = 0.75°$ are adequate to resolve the equatorially trapped coupled unstable modes.

## 3. Coupled unstable modes in the warm pool regime

### *a. A hierarchy of reduced-physics models*

In the full ocean model for warm pool system [Eq. (2.2)], three types of processes affecting SST are included: (a) turbulent entrainment, surface evaporation, and Ekman pumping in the mixed layer, which are determined, to a large extent, by surface winds; (b) shortwave radiational heating, which is controlled by the amount of cloudiness or low-level convergence; and (c) the thermocline displacement associated with ocean wave dynamics. For convenience, we will refer to the coupling associated with the above processes (a), (b), and (c) as wind-entrainment–evaporation feedback, cloud-radiation feedback, and wind–ocean wave dynamics feedback, respectively.

To identify the roles of the above three coupling processes on the coupled instability, two simplified versions

TABLE 1. Typical values of model parameters.

| | | |
|---|---|---|
| $T_r$ | Reference temperature in the deep ocean | 283 K |
| $H_1$ | Mean mixed layer depth | 40 m |
| $C_D$ | Drag coefficient | $1.5 \times 10^{-3}$ |
| $C_E$ | Moisture transfer coefficient | $1.5 \times 10^{-3}$ |
| $A$ | Surface albedo | 0.06 |
| $S_0$ | Surface solar radiation flux under clear sky | 320 W m$^{-2}$ |
| $C_a$ | Dry atmospheric internal Kelvin wave speed | 50 m s$^{-1}$ |
| $m$ | Turbulent mixing coefficient due to wind stirring | 1.25 |
| $r_s$ | Viscosity coefficient in ocean Ekman layer | $1 \times 10^{-5}$ s$^{-1}$ |
| $\varepsilon_a$ | Rayleigh friction coefficient in the atmosphere | $1 \times 10^{-6}$ s$^{-1}$ |
| $\varepsilon_o$ | Rayleigh friction coefficient in the upper ocean | $1 \times 10^{-7}$ s$^{-1}$ |
| $\mu_a$ | Newtonian damping coefficient in the atmosphere | $1 \times 10^{-6}$ s$^{-1}$ |
| $\mu_o$ | Newtonian damping coefficient in the ocean mixed layer | $1 \times 10^{-8}$ s$^{-1}$ |
| $\lambda$ | Proportionality coefficient between cloud and wind convergence | $2 \times 10^5$ s |

TABLE 2. The basic-state parameters and associated coupling coefficients in the warm pool and cold tongue regions.

| | | Warm pool | Cold tongue |
|---|---|---|---|
| $\underline{H}$ (m) | Mean thermocline depth | 150 | 70 |
| $\underline{U}$ (m s$^{-1}$) | Mean surface wind | 3 | −5 |
| $\underline{T}$ (K) | Mean SST | 303 | 299 |
| $\underline{C_a^*}$ (m s$^{-1}$) | Moist atmospheric Kelvin wave speed | 10 | 25 |
| $\underline{T} - \overline{T}_e$ (K) | Difference between $\underline{T}$ and mean entrained (upwelled) water temperature | 1.8 | 5.3 |
| $\overline{w}_e$ (m s$^{-1}$) | Mean entrainment (upwelling) rate | $2 \times 10^{-6}$ | $4.4 \times 10^{-6}$ |
| $\alpha_a$ (kg s$^{-3}$ K$^{-1}$) | Latent heating coefficient | 12 | 20 |
| $\alpha_o$ (s$^{-1}$) | Wind stress coefficient | $0.36 \times 10^{-7}$ | $1.8 \times 10^{-7}$ |
| $D_{rad}$ (K) | ML heating coeff. due to shortwave radiation | 0.2 | 0.0 |
| $D_{ent}$ (K s$^{-1}$) | ML heating coeff. due to entrainment (upwelling) | $0.9 \times 10^{-7}$ | $1.68 \times 10^{-7}$ |
| $D_{eva}$ (K s$^{-1}$) | ML heating coeff. due to evaporation | $0.72 \times 10^{-7}$ | $1.2 \times 10^{-7}$ |

of the present model were designed with a progressively reduced level of complexity in the ocean processes.

Model Ia eliminates the wind-wave dynamics feedback. For this purpose, the thermocline depth is assumed to be a constant H (the mean depth)—that is, the perturbation thermocline depth $h$ vanishes and the ocean wave dynamics *decouples* with mixed layer physics. In this *no-wave-dynamics* limit, the ocean model consists of only two mixed layer equations:

$$\frac{\partial h_1}{\partial t} = E\overline{U}U + \overline{w}_e\left(\frac{3U}{\overline{\overline{U}}} - \frac{H}{H_2}\frac{h_1}{H_1}\right) \quad \text{and} \tag{3.1a}$$

$$\frac{\partial T}{\partial t} = D_{rad}\left(\frac{\partial U}{\partial x} + \frac{\partial V}{\partial y}\right) - D_{ent}\left(\frac{3U}{\overline{\overline{U}}} - \frac{h_1}{H_1}\right) - D_{eva}\left(\frac{U}{\overline{\overline{U}}} + \frac{T}{\overline{\overline{T}} - 293}\right) - \mu_o T. \tag{3.1b}$$

Model Ib further neglects cloud-radiation feedback by taking $D_{rad} = 0$ in (3.1b). The resulting oceanic equations become

$$\frac{\partial h_1}{\partial t} = E\overline{U}U + \overline{w}_e\left(\frac{3U}{\overline{\overline{U}}} - \frac{h_1}{H_1}\right) \quad \text{and} \tag{3.2a}$$

$$\frac{\partial T}{\partial t} = -C\frac{U}{\overline{\overline{U}}} + D_{ent}\frac{h_1}{H_1} - dT, \tag{3.2b}$$

where

$$C = 3D_{ent} + D_{eva}. \tag{3.2c}$$

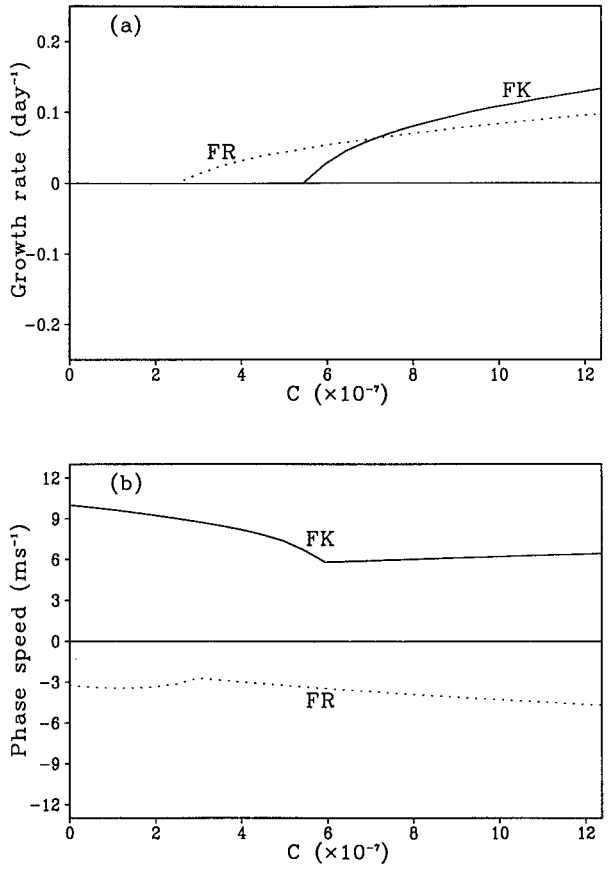


FIG. 2. Dependence of the growth rate (a) and phase speed (b) of the coupled high-frequency Kelvin (FK) and Rossby (FR) modes on wind-entrainment–evaporation coupling coefficient C (K s$^{-1}$) in model Ib of the warm pool system [Eq. (3.2)]. The atmospheric Rayleigh friction and Newtonian damping were neglected.

### *b. Unstable modes due to wind-entrainment–evaporation feedback*

Let us first examine the nature of the coupled modes in the simplest model Ib in which the change in SST is solely due to wind-induced mixed layer entrainment, evaporation, and Ekman pumping. A simple scaling indicates that the first term on the rhs of Eq. (3.2b) plays a dominant role in changing mixed layer temperature. This term represents the major portion of the wind-induced evaporation and entrainment cooling. The thermal coupling coefficient $C$ measures the degree of influence of anomalous wind-induced entrainment and surface latent heat flux on mixed layer temperature.

Figure 2 shows the growth rate of coupled unstable modes as function of thermodynamic coupling coefficient $C$. When $C$ exceeds a critical value, the mean state becomes unstable and two coupled growing modes

emerge. One propagates eastward with an average speed of 6–7 m $s^{-1}$. This mode originates from neutral atmospheric moist Kelvin wave, and, for convenience, it is referred to as coupled high-frequency Kelvin mode (CHFK) in this paper. The other propagates westward with a speed about 4–5 m $s^{-1}$. It is rooted in atmospheric moist Rossby wave and is referred to as coupled high-frequency Rossby mode (CHFR). The instability threshold value of $C$ required by coupled Rossby mode is lower than that for coupled Kelvin mode. For a typical value of $C$ ($1 \times 10^{-6}$ K $s^{-1}$), however, the coupled Kelvin mode grows faster than the coupled Rossby mode. The growth rates of the unstable modes have an $e$-folding timescale on an order of one to two weeks in the absence of dissipation. The coupling of the atmospheric wind with mixed layer entrainment and evaporation *reduces* the eastward propagation speed of the original atmospheric moist Kelvin waves (10 m $s^{-1}$), but it *increases* the westward phase speed of the original atmospheric moist Rossby waves ($-3.3$ m $s^{-1}$). The ratio $3D_{ent}/D_{eva}$ measures the relative contribution to coupled instability of evaporation vs entrainment.

Figure 3 shows the growth rate and phase speed as functions of wavenumber (wavelength) in model version Ib for the given typical value of $C$. Both the CHFK and CHFR modes prefer planetary scales. Wind–mixed layer coupling suppresses short waves. The suppression of short waves results from the feedback of SST to atmospheric waves. Shorter waves have less time to affect SST persistently when they pass over the ocean, because the perturbation wind reverses its direction more frequently. This would only yield a moderate change in SST, which in turn results in a weak feedback to wave growth. The unstable CHFK and CHFR modes are weakly dispersive as seen from the dependence of phase speed on wavelength.

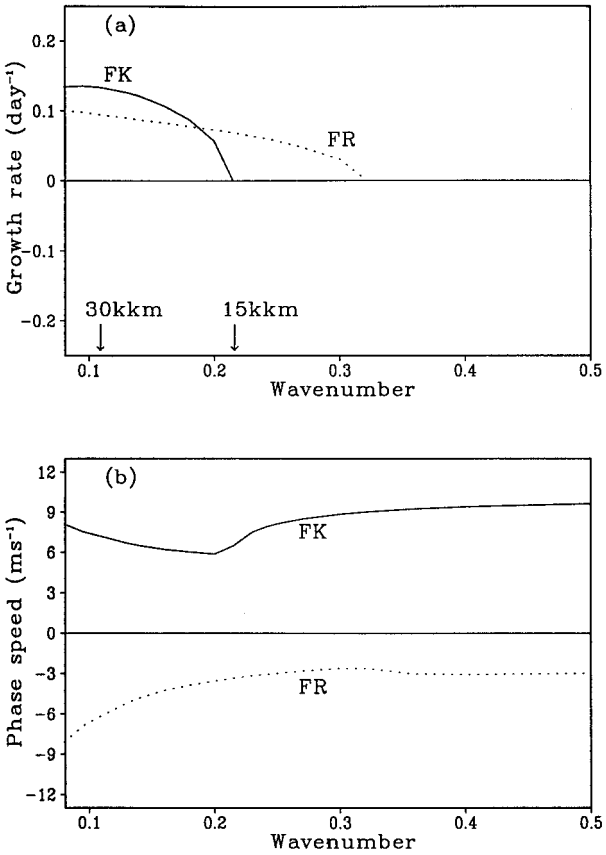


FIG. 3. The growth rate (a) and phase speed (b) of the coupled high-frequency Kelvin (FK) and Rossby (FR) modes as functions of nondimensional wavenumber for a fixed wind-entrainment–evaporation coupling coefficient $C = 1 \times 10^{-6}$ K $s^{-1}$ in model Ib. The atmospheric Rayleigh friction and Newtonian damping were neglected. The arrows with symbols ''30 kkm'' and ''15 kkm'' indicate the nondimensional wavenumbers that correspond to a wavelength of 30 000 km and 15 000 km, respectively.

### c. *Effect of cloud-radiation feedback*

In model Ia, the effect of atmospheric cloudiness on SST is included. Comparison of the results obtained from models Ia and Ib would reveal effects of cloud-radiation feedback. It turns out that the growth rate and phase speed of both the coupled unstable modes (CHFK and CHFR) are modified by cloud-radiation feedback, but their fundamental characteristics remain qualitatively unchanged.

Figure 4 displays the most unstable wavelength and corresponding growth rate and phase speed as functions of cloud-radiation feedback coefficient $D_{rad}$ and wind-entrainment–evaporation feedback coefficient $C$ for CHFK mode. When $C$ is fixed and small ($C < 3.5 \times 10^{-7}$ K $s^{-1}$), stronger cloud-radiation feedback (larger value of $D_{rad}$) yields faster growth and propagation. In particular it enhances shortwave instability. In the absence of evaporation and entrainment cooling processes ($C = 0$), the cloud-radiation feedback alone would favor the shortest CHFK mode. However, if we modify atmospheric heating representation by introducing a time lag in the latent heat release, as first suggested by Davies (1979), the shortwave instability would be effectively suppressed and longwave instability retains (figure not shown). On the other hand, for unstable CHFR mode, the cloud-radiation feedback remains favorable for planetary scales.

For a typical value of $C = 1 \times 10^{-6}$ K $s^{-1}$, the growth rate and the most unstable wavelength do not vary with $D_{rad}$ significantly until $D_{rad}$ becomes unrealistically large (say $D_{rad}$ is greater than 1 K). For typical value of $D_{rad} = 0.2$ K, the effects of cloud-radiation feedback on the most unstable wavelength, growth rate, and phase speed are moderate. This implies that the effects of wind-entrainment–evaporation feedback dominate over those of cloud-radiation feedback.

### d. *Effects of wind–ocean wave dynamics feedback*

One might wonder what would happen when ocean dynamics become progressively more important. Com-

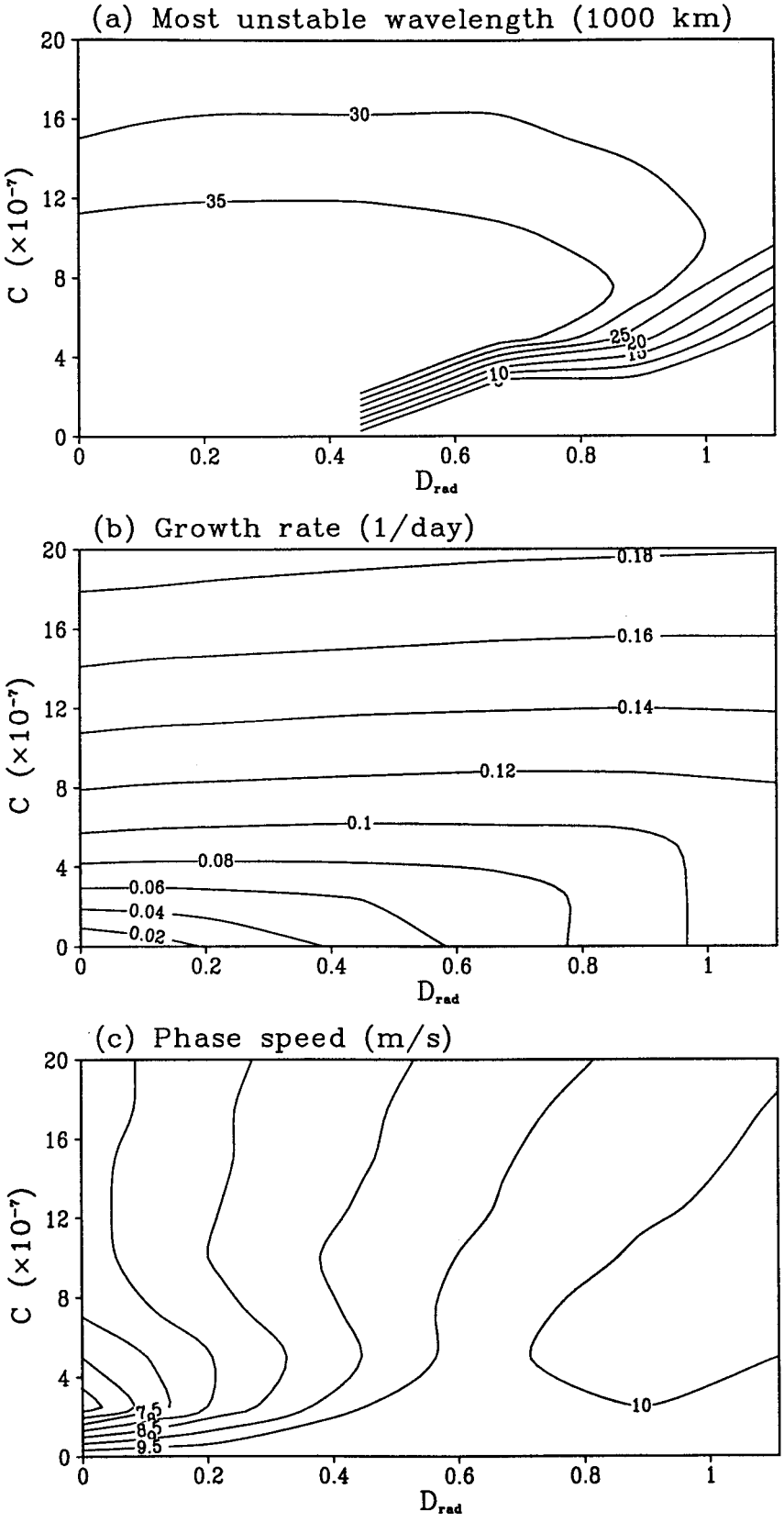
(a) Most unstable wavelength (1000 km)
30
35
25
20
15
10
C (×10⁻⁷)
D_rad
(b) Growth rate (1/day)
0.18
0.16
0.14
0.12
0.1
0.08
0.06
0.04
0.02
C (×10⁻⁷)
D_rad
(c) Phase speed (m/s)
10
7.5
8.5
9.5
C (×10⁻⁷)
D_rad

putations show that the solution obtained with the full ocean model is nearly identical to that obtained using model Ia. Evidently, for the warm pool basic state, the oceanic wave dynamics have little impact on the coupled instability.

Even when one further reduces the mean thermocline depth $H$ from 150 to 50 m in the full model, the instability of the warm pool basic state remains insensitive to change of thermocline depth or to the dynamic control of SST. No slow unstable coupled mode was found in the present model. This indicates that the wind–mixed layer thermodynamic coupling in the presence of *mean westerlies* suppresses slow unstable modes that otherwise were possibly originated from oceanic processes.

As will be shown in section 6, in an easterly mean state (the cold tongue regime), the wind–mixed layer interaction cannot suppress low-frequency unstable mode if the mean thermocline depth is sufficiently shallow (less than 100 m, for instance). The suppression of the low-frequency unstable mode by the wind–mixed layer interaction depends on the mean surface wind direction. This is because the direction of the mean surface zonal winds determines the existence of the mean upwelling or downwelling and thus determines the dominant process responsible for SST variation.

## 4. Mechanism of the coupled warm pool instability

### *a. Dynamic structure*

Figure 5 shows the horizontal structure of the unstable CHFK mode in model Ia. Similar to neutral equatorial Kelvin waves, all fields are symmetric about and trapped to the equator; the zonal winds are in geostrophic balance with the meridional pressure gradient. The low-level westerlies are no longer precisely in phase with but rather slightly lead the positive pressure (or negative thickness–temperature) anomalies. Note that the constant phase lines away from the equator tend to tilt westward and poleward. As such, the eastward propagation of the unstable mode would yield a poleward propagation component away from the equatorial region. The tilt of the constant phase line with latitude is a characteristic of unstable equatorial trapped waves. The sign change of the Coriolis force at the equator traps Kelvin waves to the equator. The trapping scale is the equatorial Rossby radius of deformation, which depends on the Kelvin wave propagation speed $C$. When the Kelvin wave becomes unstable ($C$ is complex), the trapping scale depends on the phase speed (real part of $C$), while the phase itself becomes a function of latitude. For a growing (decaying) wave, the constant phase line tilts westward (eastward) and northward. The degree of phase tilt depends on dissipation parameters and the growth rate.

For a zonal wind perturbation with an amplitude of 2 m $s^{-1}$, the corresponding amplitude of SST perturbation is about 0.3°C. The SST response associated with the CHFK mode is thus substantially stronger than that in Hirst and Lau's (1990) intraseasonal mode (by a factor of 3). This suggests the importance of thermodynamic coupling of the atmosphere and ocean mixed layer. The ratio of magnitude between SST and surface wind anomalies appears to be reasonable compared to COARE observations. The latter show that after strong westerly burst episodes (amplitude is about 10 m $s^{-1}$), SST drops about 2°C on an intraseasonal timescale (Lau and Sui 1997).

The phase relationship between atmospheric fields and mixed layer temperature (or SST) is particularly interesting for the coupled mode. For the growing CHFK mode, positive SST anomalies lead low-level convergence and rainfall by about two-tenths of a cycle (or about 70° in phase) (Fig. 5b). This phase shift results primarily from competitive effects of two processes. On the one hand, westerly anomalies augment mean westerlies, thus enhancing evaporation and entrainment cooling in the ocean mixed layer. This process alone would tend to make westerly anomalies lead negative SST anomalies by a quarter of a wavelength. On the other hand, the enhanced convection tends to reduce net downward shortwave radiation flux and to cool mixed layer water. The cloud-induced cooling region tends to be located a quarter wavelength to the west of convection anomalies and thus roughly coincide with the surface westerly anomalies. As a result of the combined influences from the above two processes, the negative SST anomalies slightly lag the anomalous westerlies. Meanwhile, positive SST anomalies lead enhanced convection by about 70° in phase. Mixed layer deepening also lags anomalous westerlies by about 70° in phase (Fig. 5c), because the westerlies tend to deepen mixed layer via Ekman divergence-induced downwelling while the entrainment-induced mixed layer depth fluctuation is of secondary importance.

### *b. The energy conversion for coupled unstable modes*

To facilitate interpretation of the coupled instability, it is useful to examine energy conversion. Let us focus on the atmospheric perturbation of the coupled mode. Define ensemble mean atmospheric eddy kinetic energy per unit mass as $K_a = \overline{(U^2 + V^2)}/2$, and atmospheric eddy available potential energy as $P_a = \overline{\phi^2}/2C_a^2$. Use an overbar to represent horizontal average over a zonal

←

FIG. 4. The wavelength (a), growth rate (b), and phase speed (c) of the most unstable mode as functions of the cloud-radiation coupling coefficient $D_{rad}$ (K) and wind-entrainment–evaporation coupling coefficient $C$ (K $s^{-1}$) for the coupled high-frequency Kelvin mode in model Ia.

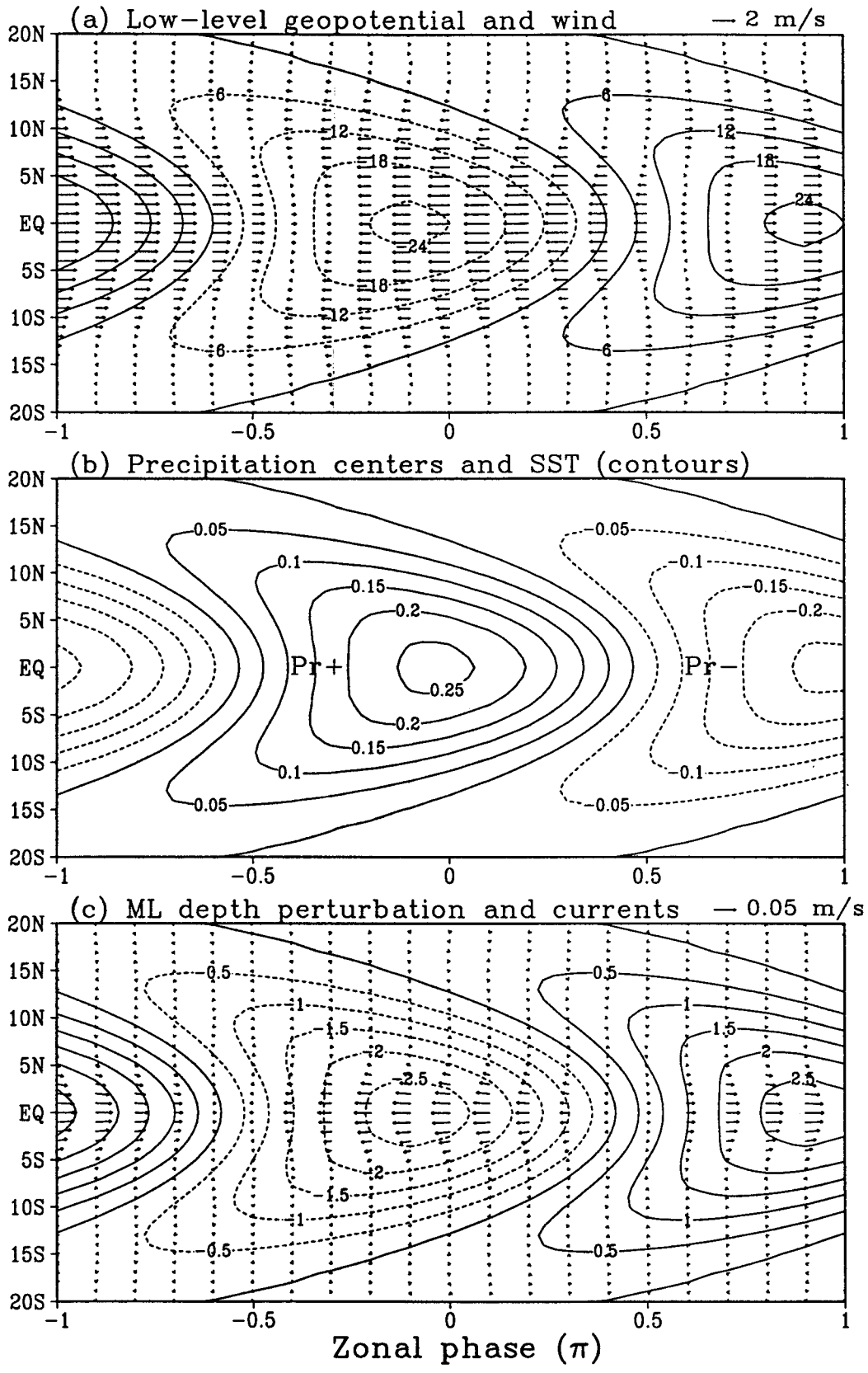
(a) Low−level geopotential and wind
— 2 m/s
(b) Precipitation centers and SST (contours)
Pr+
Pr−
(c) ML depth perturbation and currents
— 0.05 m/s
20N
15N
10N
5N
EQ
5S
10S
15S
20S
−1
−0.5
0
0.5
1
Zonal phase (π)

wavelength and from $y = -Y_b$ to $y = Y_b$, where $-Y_b$ and $Y_b$ denote southern and northern boundaries of the coupled model, respectively. The following energy equations can be derived from Eqs. (2.1):

$$\frac{\partial K_a}{\partial t} = \langle P, K\rangle - 2\varepsilon_a K_a, \tag{4.1a}$$

$$\frac{\partial P_a}{\partial t} = \langle P, K\rangle + GP_1 + GP_2 - 2\mu_a P_a, \tag{4.1b}$$

where

$$\langle P, K\rangle = \overline{\phi\left(\frac{\partial U}{\partial x} + \frac{\partial V}{\partial y}\right)}, \tag{4.2a}$$

$$GP_1 = \overline{I\phi\left(\frac{\partial U}{\partial x} + \frac{\partial V}{\partial y}\right)}, \quad \text{and} \tag{4.2b}$$

$$GP_2 = -\frac{\alpha_a}{C_a^2}\overline{T\phi}. \tag{4.2c}$$

The term $\langle P, K\rangle$ denotes conversion from atmospheric eddy available potential energy (EAPE) to kinetic energy. Here, $GP_1$ denotes generation rate of atmospheric EAPE due to condensational heating associated with low-level moisture convergence, which depends on the covariance between low-level moisture convergence and atmospheric temperature anomaly, while $GP_2$ is the generation rate of atmospheric EAPE due to the heating induced by SST anomalies, which depends on the covariance between SST and atmospheric temperature anomalies.

The structure of the unstable CHFK mode indicates a favorable energy conversion for the unstable mode. Because low-level convergence and convective rainfall tend to overlap with positive temperature (negative geopotential in the lower troposphere) anomalies, a positive covariance between temperature anomalies and low-level convergence-induced heating results in a generation of EAPE [the $GP_1$ term in Eq. (4.1b); Fig. 6a], which is further converted to perturbation kinetic energy.

Note that the $GP_1$ term alone is insufficient for unstable growth because it is smaller than $\langle P, K\rangle$ (Fig. 6b). That means the atmosphere is dynamically stable in the absence of a coupling to the ocean. It is the additional $GP_2$ term that makes the CHFK mode grow. The term $GP_2$, which is proportional to the covariance between negative low-level pressure and positive SST anomalies [Eq. (4.2c)], is due to the atmospheric heating associated with SST perturbation. For growing CHFK mode, positive SST and negative low-level pressure anomalies are positively correlated. This yields generation of EAPE (Fig. 6c) and the development of the CHFK mode. It is clear that the atmosphere–ocean mixed layer interaction is responsible for the unstable CHFK mode in the present model.

A parallel analysis for the ocean component shows that the SST perturbation is amplified by wind-entrainment–evaporation feedback—that is, the SST perturbation grows when the westerly (easterly) anomalies and negative (positive) SST anomalies have a positive covariance. This is indeed the case for the CHFK mode.

The atmospheric component of the unstable CHFR mode displays a structure similar to that of $m = 1$ Rossby wave, where m is an index for meridional mode (Fig. 7a). Strong westerly anomalies are associated with twin cyclones residing on both sides of the equator. Rainfall areas are located not only at the equator but also at the off-equatorial region. The off-equatorial rainfall regions lag positive SST anomalies by about 60°, while the equatorial rainfall region is nearly in phase with positive SST anomalies. The generation of atmospheric EAPE due to air–sea coupling is primarily in the off-equatorial regions where the low-level low pressure is strongly correlated with positive SST anomalies (figure not shown).

## 5. Coupled modes of the cold tongue regime

Over the equatorial eastern Pacific, the ocean dynamics have an essential control on SST variation, whereas entrainment and diabatic heating processes in the mixed layer are of secondary importance. The governing equations for the perturbation motion in the cold tongue regime are (see appendix)

$$\frac{\partial u}{\partial t} - \beta y v = -b\frac{\partial h}{\partial x} + \alpha_o U - \varepsilon_o u, \tag{5.1a}$$

$$\frac{\partial v}{\partial t} - \beta y u = -b\frac{\partial h}{\partial y} + \alpha_o V - \varepsilon_o v, \tag{5.1b}$$

$$\frac{\partial h}{\partial t} + H\left(\frac{\partial u}{\partial x} + \frac{\partial v}{\partial y}\right) = 0, \quad \text{and} \tag{5.1c}$$

$$\frac{\partial T'}{\partial t} = D_{up}\frac{h'}{H_2} + D_{rad}\left(\frac{\partial U}{\partial x} + \frac{\partial V}{\partial y}\right) - (D_{up} + D_{eva})\frac{U}{\overline{U}} - \tilde{\mu}_o T', \tag{5.1d}$$

where coefficients $D_{up}$ and $\tilde{\mu}_o$ are defined by Eqs. (A.8a,b). The atmospheric equations are the same as Eqs. (2.1a)–(2.1c).

For convenience, the model equations (5.1a)–(5.1d)

←

FIG. 5. Horizontal structure of the coupled unstable high-frequency Kelvin mode in model Ia: (a) low-level geopotential (contour interval 6 $m^2\ s^{-2}$) and winds; (b) SST (°C) anomaly and anomalous precipitation centers denoted by $P_{r+}$ and $P_{r-}$; (c) mixed layer depth (m) and current anomalies.

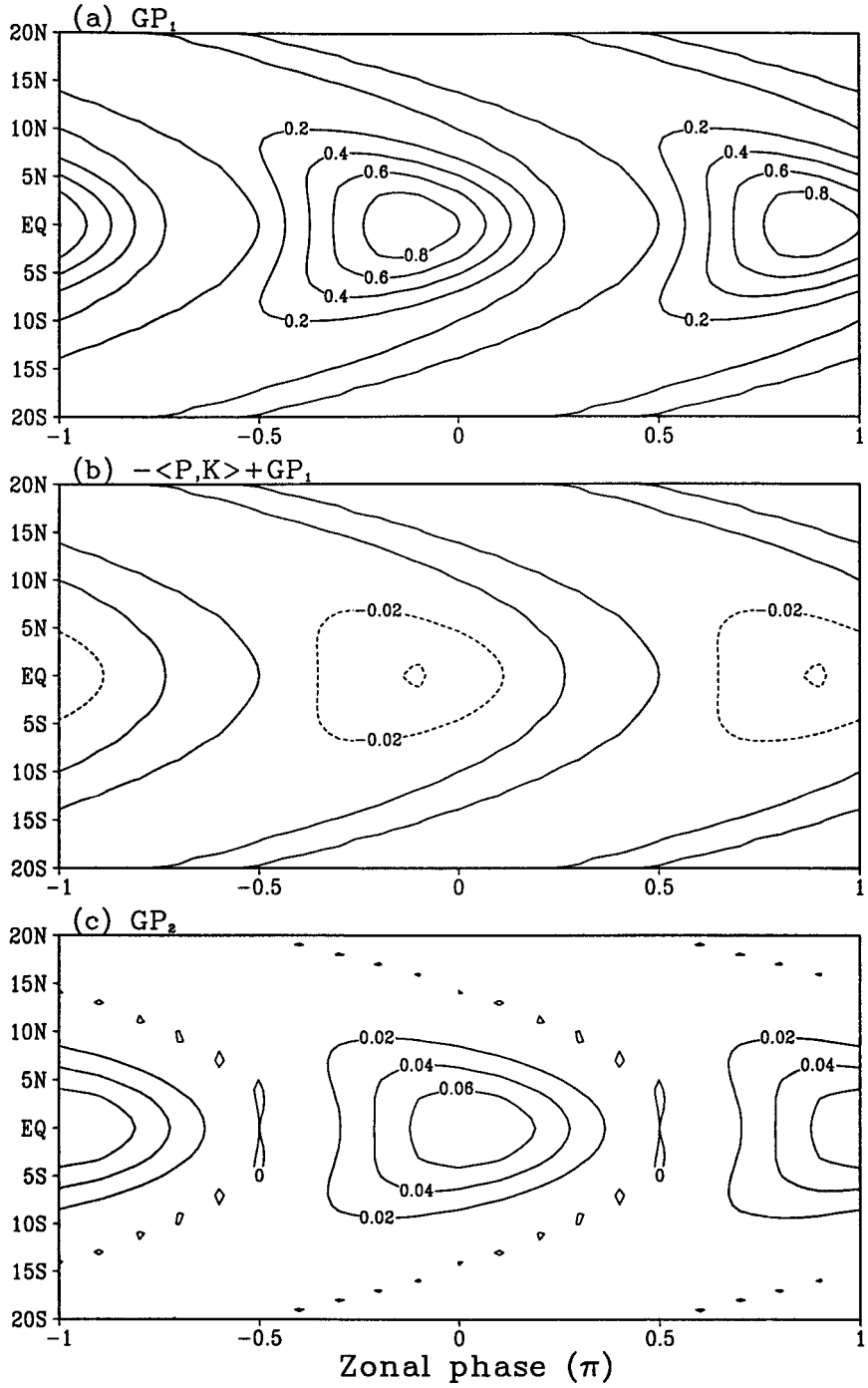


FIG. 6. The rate of energy generation for the most unstable coupled high-frequency Kelvin mode in model Ia. (a) Eddy available potential energy (EAPE) generation due to condensational latent heating induced by moisture convergence ($GP_1$); (b) the difference between $GP_1$ and the conversion from EAPE to kinetic energy, $\langle P, K\rangle$; and (c) EAPE generation due to heating associated with SST anomaly ($GP_2$). All quantities are normalized by $\langle P, K\rangle$.

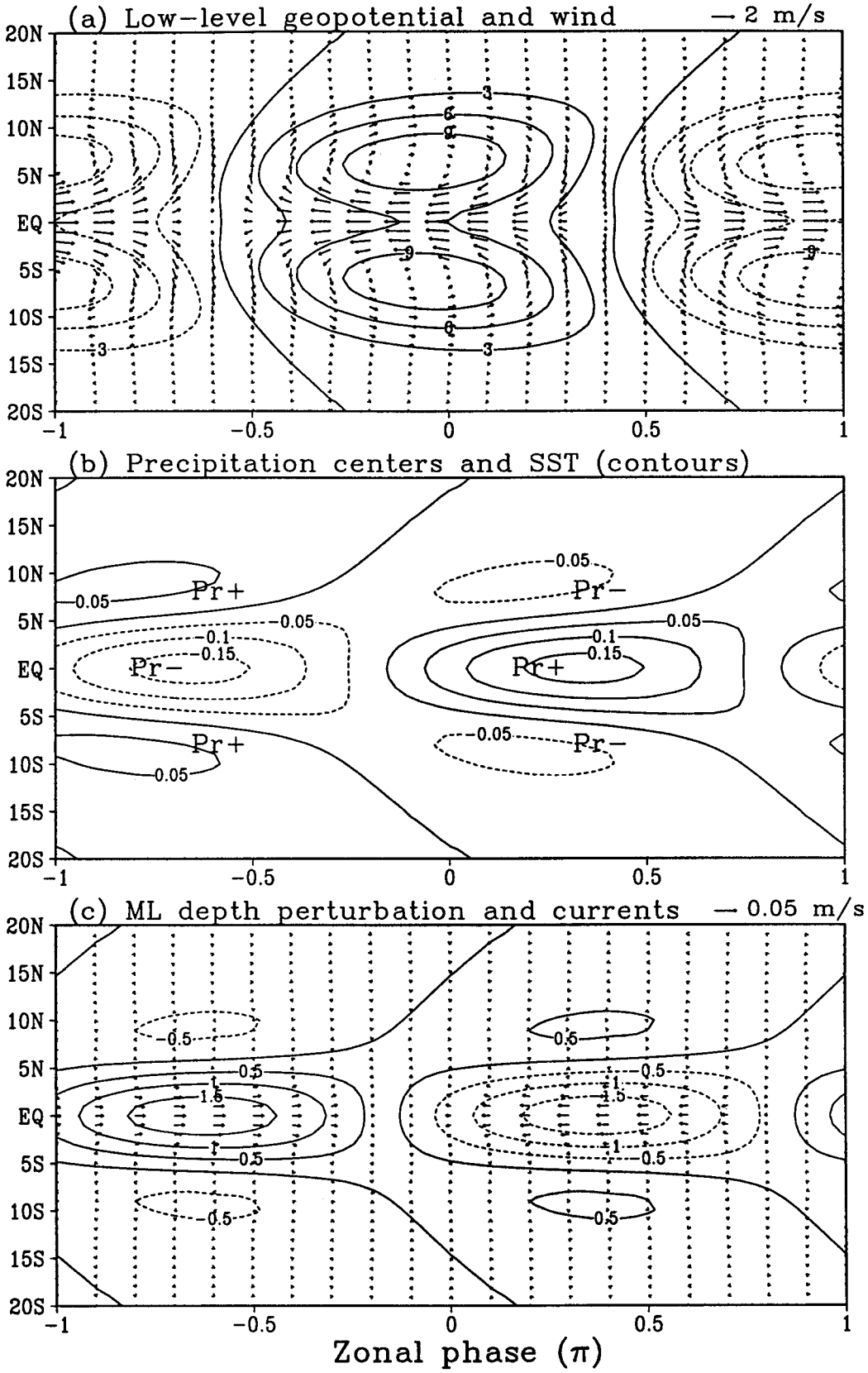


FIG. 7. The same as in Fig. 5 except for the coupled high-frequency Rossby mode.

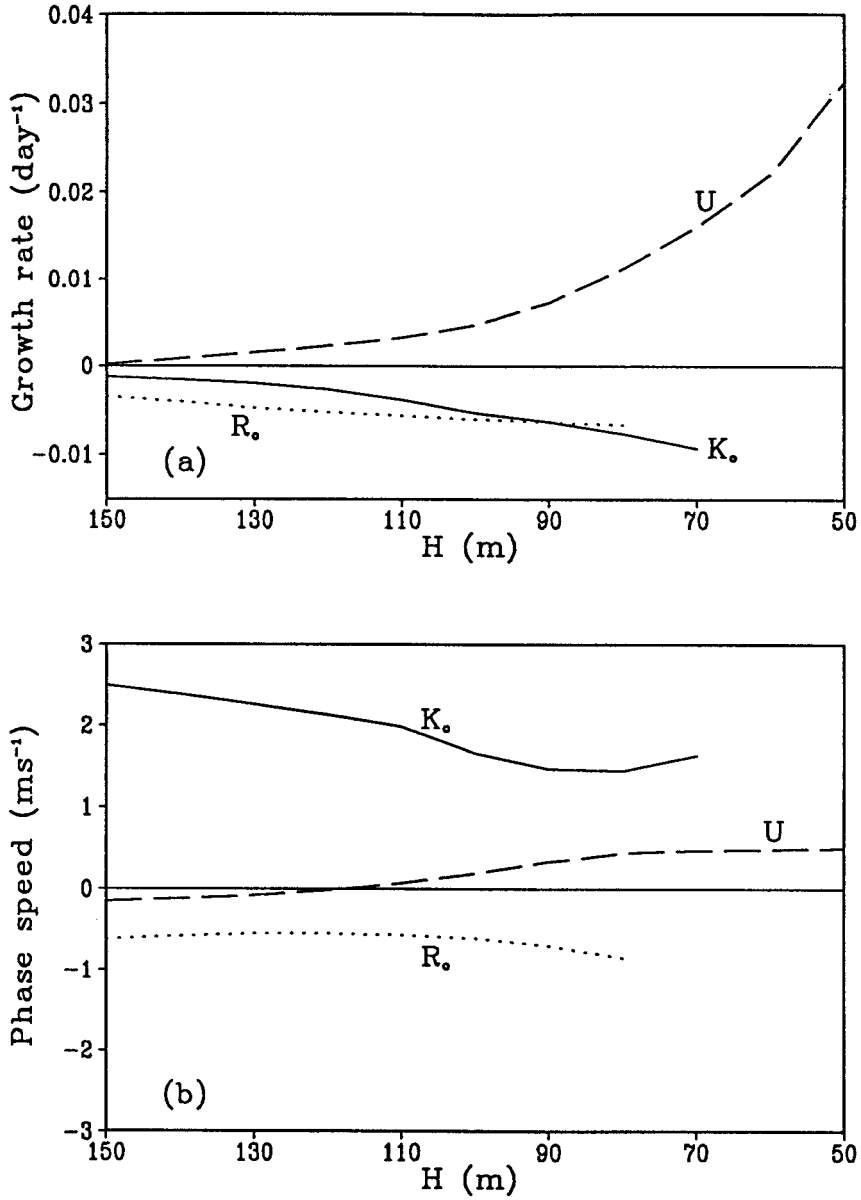


FIG. 8. Dependence of the growth rate (a) and phase speed (b) of the coupled modes on thermocline depth $H$ (m) in the cold tongue regime computed from model IIa. Symbols $U$, $K_o$, and $R_o$ denote coupled low-frequency SST mode, Kelvin mode, and Rossby mode, respectively.

are referred to as version IIa. If the diabatic heating term is further neglected, Eq. (5.1d) reduces to

$$\frac{\partial T'}{\partial t} = D_{\text{up}}\left(\frac{h'}{H_2} - \frac{T'}{\overline{\overline{T}} - T_r} - \frac{U'}{\overline{\overline{U}}}\right). \tag{5.2}$$

For convenience, the set of Eqs. (5.2) and (5.1a)–(5.1c) is called model IIb, which is essentially a simplified linear version of Zebiak and Cane's (1987) coupled model.

In contrast to the warm pool regime, the cold tongue mean state (Table 2) supports coupled unstable modes, which are associated with oceanic processes and have a longer timescale. In model IIa, oceanic waves (Kelvin and Rossby waves) remain damped in the presence of ocean–atmosphere interaction and dissipation (Fig. 8a). There is only one unstable mode that owes its origin to thermodynamic processes. This result agrees well with the result of Hirst (1986), although the model here is slightly different from his. Neelin (1991) named this type of unstable mode slow SST mode. It is originated from the vertical temperature advection associated with upwelling process, while the horizontal temperature advection may slightly modify this mode (Hirst 1986).

The growth rate of the unstable SST mode increases

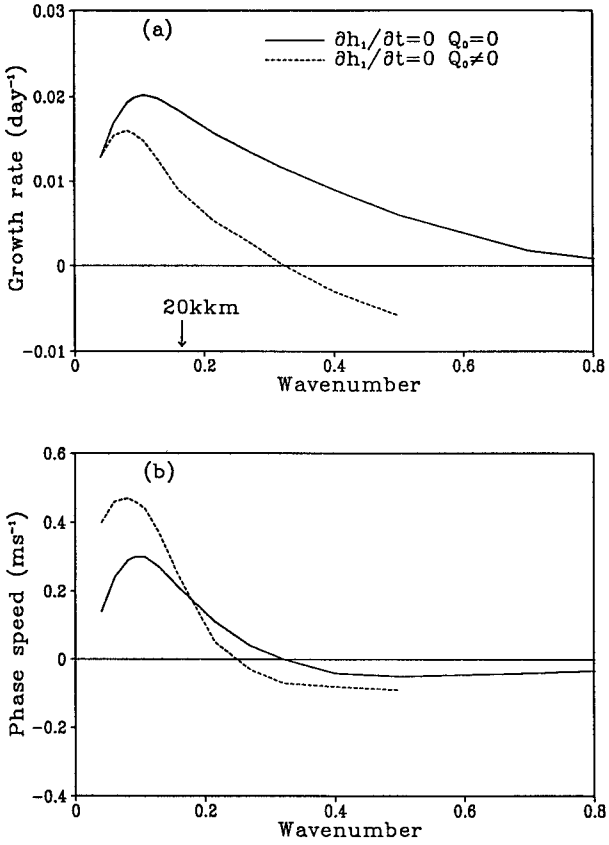


FIG. 9. The growth rate (a) and phase speed (b) of the low-frequency unstable SST mode as functions of nondimensional wavenumber. The atmospheric Rayleigh friction and Newtonian cooling coefficients used are $\varepsilon = \mu = 2 \times 10^{-6}$ s$^{-1}$. The arrow with symbol "20 kkm" indicates the nondimensional wavenumber that corresponds to a wavelength of 20 000 km.

with decreasing mean thermocline depth in model IIa (Fig. 8a). When the thermocline is deeper than about 120 m, the coupled instability is very weak and the unstable mode propagates westward slowly ($<$10 cm s$^{-1}$) (Fig. 8b); when the mean thermocline is shallower than about 90 m, the growth rate corresponds to an *e*-folding time of about 150 days and the unstable mode propagates eastward with a faster speed (20–30 cm s$^{-1}$).

Comparison of the results obtained from model IIa and IIb indicates that, without surface heat flux exchange, the SST mode grows relatively fast (the solid curve in Fig. 9a) with a reduced most unstable wavelength. The eastward propagating speed for long waves (longer than 20 000 km) is much reduced. The unstable waves shorter than 10 000 km move westward. The SST mode is dispersive.

The structure of the unstable SST mode obtained in model IIa is almost the same as that of the ocean thermal mode obtained by Hirst and Lau (1990) in their model IV (figure not shown). In contrast to the CHFK mode, the SST anomalies associated with the slow SST mode are nearly in phase with rainfall, whereas the positive SST anomalies lead westerly anomalies by only one-eighth of the cycle.

The coupled high-frequency modes, which are unstable in the warm pool regime, are suppressed in the cold tongue regime. This is true not only with the model II, but also with the full model (figure not shown). Sensitivity experiments reveal that the suppression of high-frequency coupled modes is due to the increase of atmospheric static stability in the cold tongue and due to the reversal of the mean surface wind direction from westerly to easterly. The development of CHFK mode crucially depends on both the mean surface westerlies and the reduced atmospheric static stability, whereas the unstable CHFR mode requires only the latter.

## 6. Roles of air–sea interaction in maintaining Madden–Julian Oscillation

TOGA COARE has provided an unprecedented opportunity to observe the behavior of MJO and accompanying oceanic variations. Figure 10a presents a concise summary of the results obtained from recent empirical studies.

The structure of MJO in the equatorial zonal plane consists of a wet and a dry phase. The wet phase features a large-scale convective envelope whose core consists of super cloud clusters—an ensemble of two-day waves and mesoscale convective systems (Chen et al. 1996; Sui et al. 1997). The convective region is accompanied by large-scale rising motion and planetary-scale, equatorial upper-level easterly and low-level westerly anomalies (Lin and Johnson 1996). The low-level (and surface) westerly anomalies, however, lag behind enhanced convection by slightly less than a quarter-wavelength (e.g., Chen et al. 1996; Chou et al. 1995). This concurs with the result of Fasullo and Webster (1995), who found that 850-hPa zonal winds lag rainfall and maximum cloud optical depth by a temporal phase of about a week. The above vertical structure agrees well with the composite structure of MJO previously documented by Rui and Wang (1990), Salby and Hendon (1994), and Hendon and Salby (1994).

A number of new features concerning the phase relationship between MJO and upper-ocean variations have been revealed, which are critical to understanding the dynamics of MJO and to validating current theories. First, the surface latent heat flux associated with MJO exhibits pronounced longitudinal asymmetries: Enhanced evaporation anomalies almost coincide with low-level westerly anomalies, whereas reduced latent heat flux is found to be nearly in phase with easterly anomalies (Jones and Weare 1996; Zhang 1996; Lin and Johnson 1996). This feature contradicts the premise that strong latent heat flux occurs in the easterly phase of MJO due to the presence of basic-state easterlies. Thus, theories based on this premise cannot explain the eastward propagation of MJO (Wang 1988b). Second, the positive SST anomalies lead enhanced convection by

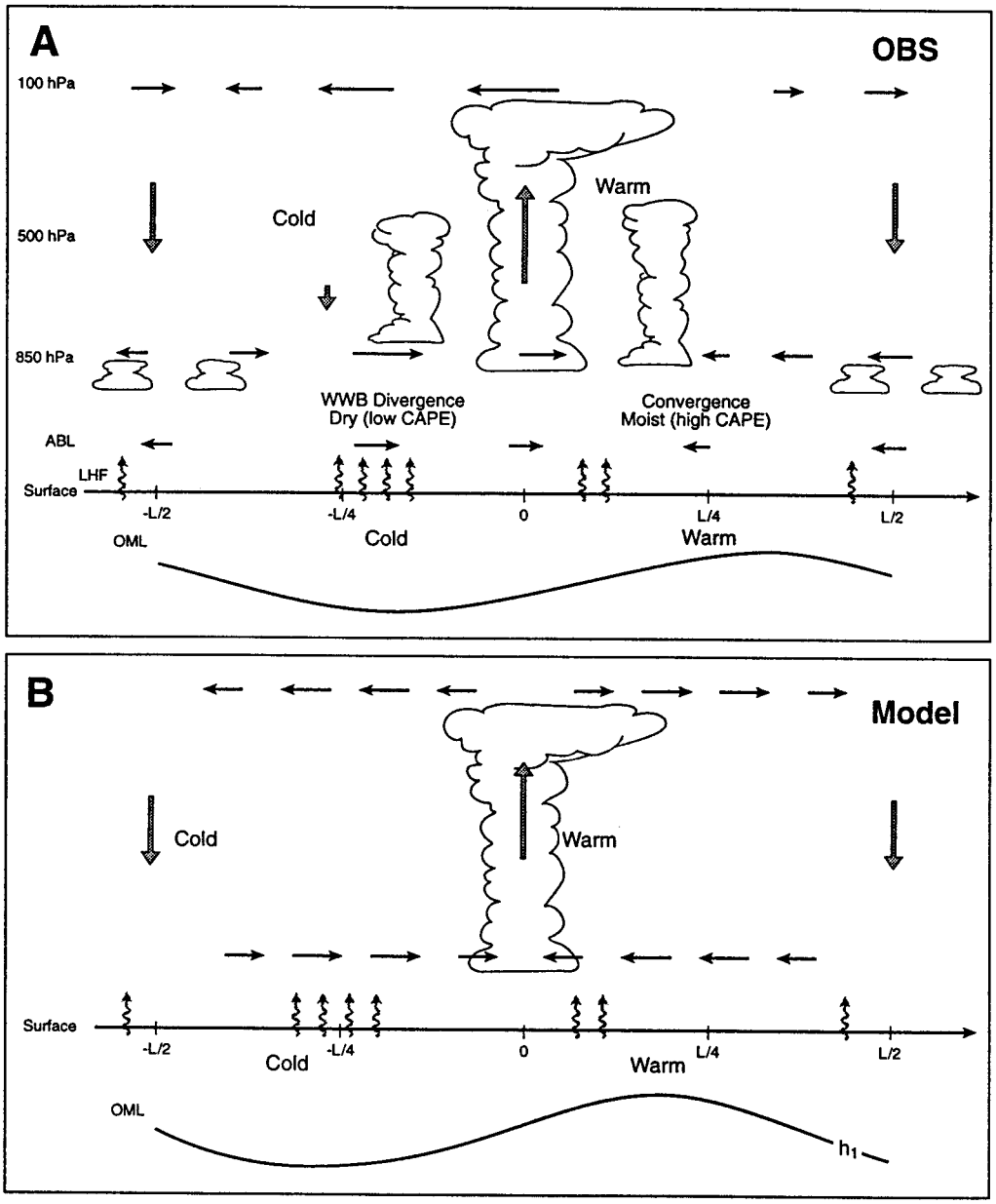


FIG. 10. Schematic diagram illustrating the equatorial vertical structure of the Madden–Julian Oscillation observed in TOGA COARE (a) and the coupled high-frequency Kelvin mode in the present model (b). The squiggly lines denote surface latent heat flux. The symbols ABL, OML, LHF, WWB, CAPE, and L represent, respectively, atmospheric boundary layer, ocean mixed layer, latent heat flux, westerly wind bust, convective available potential energy, and wavelength. The observations are based on the results obtained by Chen et al. (1991), Sui et al. (1996), Zhang (1996), Lin and Johnson (1996), Jones and Weare (1991), Fasullo and Webster (1995), and Chou et al (1995).

slightly less than a quarter of a wavelength. This is in good agreement with the previous results derived from COADS analyses (Kawamura 1988). The present model analysis has explained what is responsible for this phase lead and what roles this phase lead plays in supporting coupled instability.

The dynamic structure of the most unstable CHFK mode, which results from the coupled instability of warm pool mean state, is shown in Fig. 10b. This schematic figure is based on the model results shown in Fig. 5. The overall structure of the CHFK mode resembles that of the MJO and, in particular, the phase relationship between atmospheric circulation and SST. However, the phase relationship between the convection and low-level westerlies is not well captured by the model. This appears to be a common weakness of the current theoretical models of the MJO. In addition to the similarity in the dynamic structure, the preferred wavelength and

slow eastward propagation of the CHFK mode also bear close resemblance to the MJO. The similarities between the CHFK mode and the observed MJO in the phase relationships between atmospheric and ocean mixed layer anomalies further add confidence to the relevance of the CHFK mode to the MJO. Thus, the behavior of the CHFK mode may be instrumental for understanding some of the observed features of the MJO.

Previous theories of the MJO have been based on atmospheric internal dynamics without invoking variations in the ocean mixed layer. Convective interaction with large-scale atmospheric dynamics has been recognized as a key element of the theoretical modeling of the MJO. Although these models reproduced some observed features of the MJO, a fundamental difficulty is the lack of planetary wave selection mechanism. The simulated eastward propagation in many models tends to be much faster than that observed.

The present model results suggest a new mechanism for the MJO that is complimentary to the mechanism of atmospheric internal dynamic instability. The new mechanism involves atmosphere–ocean mixed layer interaction through thermodynamic processes. It is demonstrated that the wind–cloud–mixed layer coupling via changing entrainment rate, latent heat, and shortwave radiation fluxes renders growing SST perturbation and, in particular, makes positive SST anomalies lead low-level enhanced convection by about $(2/5)\pi$. There is a significant feedback from ocean mixed layer to atmospheric moist wave dynamics. The feedback may play three important roles in sustaining MJO: to provide an energy source for the amplification of atmospheric Kelvin waves, to select planetary-scale most unstable modes, and to considerably reduce their eastward propagation speed (by about one-third), which helps to match the MJO timescale (40–50 days).

Without the coupling to ocean mixed layer, the present model atmosphere has no internal unstable modes. It is the atmosphere–mixed layer thermodynamic coupling that destabilizes atmospheric moist Kelvin waves. The phase leading of SST to enhanced convection creates a positive covariance between SST and atmospheric temperature anomalies, which generates EAPE for the growing CHFK mode. Observations have shown that the equatorial Indian Ocean and the western Pacific Ocean are two major regions where the intraseasonal convective anomalies intensify (Wang and Rui 1990). This geographic preference for MJO development may be interpreted as a result of the contribution of atmosphere–ocean interaction to the MJO.

The relatively slow response of the ocean mixed layer to wind anomalies favors amplification of planetary-scale waves. This provides a natural wave selection mechanism for the MJO. Note that the coupled CHFK mode of the warm pool system involves only a coupling to shallow ocean mixed layer. The existence of maritime continent is thus not a fundamental barrier for the MJO to interact with ocean over the entire domain of the equatorial Indian and western Pacific Oceans. The longitudinal scale of the warm pool may limit the zonal scale of the coupled mode, yielding the observed wavenumber 2 structure in the realistic warm pool geography.

The presence of the maritime continent, on the other hand, may reduce the strength of the MJO through a number of processes: (a) reducing the coupled instability by prohibiting air–sea interaction; (b) raising the level of maximum latent heat release (due to land surface heating effect), which weakens the interaction between convective heating and atmospheric Kelvin waves (e.g., Miyahara 1987); (c) decreasing availability of moisture supply due to continuing release of energy during the enhanced diurnal rainfall; and (d) increasing surface dissipation over the island topography. The above arguments may explain why the maritime continent is a region of destruction to the intensity of intraseasonal convective anomalies (Rui and Wang 1990).

The behavior of the coupled unstable Rossby waves may be relevant to the observed westward propagating intraseasonal mode. In boreal summer, there is an intraseasonal mode that moves westward along 15°N in the western Pacific (Murakami 1980; Chen and Murakami 1988; Nitta 1987). This mode appears to originate from moist Rossby waves interacting with convective heating and the underlying SST. When an equatorial eastward propagating convective complex reaches the central Pacific where SST decreases sharply, the anomalous circulation tends to decouple with the convective heating and decays; meanwhile the Rossby waves emanate from the equatorial disturbance in the western North Pacific and move westward to the South Asian monsoon region (Wang and Xie 1997).

## 7. Summary

The basic state and air–sea interaction processes differ fundamentally between the warm pool of the Indian and western Pacific Oceans and the cold eastern Pacific. This leads to the following hypothesis: The nature of the coupled ocean–atmosphere instability over the warm pool may essentially differ from that of the equatorial cold tongue.

To test this hypothesis, a linear coupled ocean–atmosphere model is advanced that emphasizes ocean mixed layer physics and thermodynamic coupling of the atmosphere and ocean. These processes are believed to be relevant to the warm pool system. For completeness, the model also includes ocean wave dynamics. Different features of the ocean model are reflected in the following mixed layer processes: (i) diabatic heating due to cloud-dependent solar radiation, wind-dependent evaporation, and entrainment cooling; and (ii) the impact on SST of mixed layer depth variation, which is caused by both the surface momentum and heat flux forcing and the thermocline variation associated with the ocean dynamic processes.

The major findings of the coupled model analysis follow.

(a) In the presence of a full (dynamic and thermodynamic) coupling or in the presence of both the ocean wave dynamics and mixed layer physics, distinctive unstable coupled modes exist, depending on the basic state. The warm pool regime with a deep thermocline and weak mean surface westerlies promotes high-frequency (intraseasonal) coupled unstable modes (the coupled Kelvin and Rossby modes), whereas it prohibits low-frequency unstable SST mode. In sharp contrast, the eastern Pacific regime, in which the thermocline is shallow and surface mean winds are strong easterlies, supports a low-frequency unstable SST mode, whereas it suppresses the high-frequency coupled instability.

(b) The coupled high-frequency modes originate from atmospheric moist Kelvin and Rossby waves. They are destabilized by thermodynamical coupling to ocean mixed layer processes. The wind–mixed layer feedback via entrainment and surface evaporation plays a central role and favors planetary-scale unstable modes. The cloud effect on solar radiation selects long waves only when a time delay in the parameterized cumulus heating is included. Unstable atmospheric Rossby waves prefer planetary scales under both the wind-entrainment–evaporation feedback and the cloud-radiation feedback.

(c) The destabilization of the moist atmospheric waves by wind-entrainment–evaporation feedback depends on the direction of the basic-state winds. Only westerlies render the coupled mode unstable. The ocean wave dynamics, on the other hand, have little effect on coupled instability, even when thermocline depth is artificially reduced to one-third of the observed value.

(d) The atmosphere–ocean mixed layer thermodynamic coupling creates a significant positive covariance between the rising SST and atmospheric warming, which allows unstable modes to gain available potential energy. Second, the relatively slow response of the ocean mixed layer to anomalous wind forcing favors amplification of planetary-scale waves and significantly slows down eastward propagation of the unstable CHFK mode.

(e) The characteristics of the coupled high-frequency mode of the warm pool system compares favorably with the observed MJO. It is suggested that, in addition to the atmospheric internal dynamic instability, the ocean mixed layer thermodynamic processes interacting with the atmosphere may play a significant role in maintenance of the MJO. The air–sea thermodynamic coupling furnishes eddy energy, provides a natural wave selection mechanism, slows down atmospheric Kelvin wave propagation, and sets up a 40–50-day oscillation period for MJO.

While the mean state of the warm pool system is unstable to intraseasonal perturbations, the mean state of the cold tongue supports low-frequency SST mode. This was demonstrated using a reduced physics model IIa, which is essentially equivalent to a simplified linear model of Zebiak and Cane (1987).

For analytical simplicity and clarity, we have made a number of critical simplifications in the present model. The conclusions derived from this model are, therefore, subject to limitations of the simplified model physics. Some of the neglected physical processes are by no means always unimportant. For instance, the penetrated solar radiation and rainfall effects in the mixed layer that could be important in the mixed layer heat balance were neglected. One should also be cautious about the specific conclusions derived with the constraints of the model's formulation. For instance, in the description of the atmospheric heating, the surface wind–dependence of the latent heat flux, which certainly plays an active role in the coupled instability, was neglected. To focus on the role of atmosphere–ocean interaction and to compare the warm pool instability with the eastern Pacific instability, we have, in this part of the paper, deliberately excluded the instability mechanism internal to the atmosphere. We were, therefore, unable to examine the coupled instability, which interacts with atmospheric internal instability. This, however, is a very important issue. In view of its complexity and importance, we will address this issue specifically in Part II of the present paper.

Since the coupled modes in both the warm pool and cold tongue regimes have preferred planetary scales, it would be more realistic to examine the nature of coupled unstable modes in a spatially varying basic state including both the warm pool and cold tongue conditions and both the thermodynamic and dynamic coupling between the atmosphere and ocean.

*Acknowledgments.* We would like to thank Dr. H. Hendon and two anonymous reviewers for their constructive comments and Dr. N. Nicholls for his conscientious editorial work on a previous version of the manuscript. This research has been supported by the Climate Dynamics Program, National Science Foundation and TOGA COARE under Grant ATM 96-13776. This is the SOEST (School of Ocean and Earth Science and Technology) Publication 4637.

## APPENDIX

## Derivation of Linearized Ocean Model

### *a. Governing equations*

The ocean model was distilled from the two-and-one-half layer ocean model of Wang et al. (1995), which combines the reduced-gravity upper-ocean dynamics (Cane 1979) and the mixed layer physics. The major simplifications include (i) linearization of momentum and mass continuity equations; (ii) neglect of horizontal advection of temperature, horizontal variation of buoyancy, and penetrative shortwave radiation flux at the base of the mixed layer. The equations governing the

vertical mean upper-ocean velocity $\mathbf{v}$, the thermocline depth $h$, and the mixed layer depth $h_1$ and temperature $T$ on an equatorial $\beta$ plane are

$$\frac{\partial \mathbf{v}}{\partial t} + \beta y \mathbf{k} \times \mathbf{v} = -b\nabla h + \frac{\tau_0}{\rho_o H} - \varepsilon_o \mathbf{v}, \quad \text{(A.1a)}$$

$$\frac{\partial h}{\partial t} + H\nabla \cdot \mathbf{v} = 0, \quad \text{(A.1b)}$$

$$\frac{\partial h_1}{\partial t} + H_1 \nabla \cdot \mathbf{v}_1 = w_e, \quad \text{and} \quad \text{(A.1c)}$$

$$\frac{\partial T}{\partial t} = -\frac{w_e}{h_1}\delta(w_e)(T - T_e) + \frac{Q_0}{\rho_o c_w h_1}, \quad \text{(A.1d)}$$

where $b$ is the buoyancy; $\varepsilon_o$ the Rayleigh damping coefficient in the upper ocean; $H_1$ and $H$ denote the mean depths of the mixed layer and thermocline, respectively; $H_2 = H - H_1$; $\rho_o$ and $c_w = 4186$ J kg$^{-1}$ K$^{-1}$ the density and heat capacity of water, respectively; the wind stress at the ocean surface is estimated using the bulk aerodynamic formulas: $\tau_0 = \rho_a C_D |\overline{U}|\mathbf{V}$; and $\delta(w_e)$ is a Heaviside function of entrainment velocity $w_e$.

The mixed layer divergence, $\nabla \cdot \mathbf{v}_1$, as demonstrated by the scale analysis of Wang and Fang (1996), is primarily due to the Ekman flow, $\mathbf{v}_e$, which satisfies a balance among the wind stress, the Coriolis force, and a Rayleigh friction in the mixed layer (Zebiak and Cane 1987). After neglect of the minor influences of the meridional surface wind stress and wind divergence on Ekman pumping, one can show:

$$\nabla \cdot \mathbf{v}_1 = \frac{H_2}{H}\nabla \cdot \mathbf{v}_e = -\frac{E}{H_1}|\overline{U}|U, \quad \text{(A.1e)}$$

where $U$ is atmospheric zonal wind at the surface, the Ekman coefficient is

$$E = \rho_a H_2 C_D \beta / \rho_o H r_s^2, \quad \text{(A.1e}'\text{)}$$

and the eddy viscosity coefficient $r_s$ in mixed layer is treated as a constant.

The entrainment velocity, $w_e$, is parameterized by the mixed layer model of Niiler and Kraus (1977) upon neglect of the generation of turbulent kinetic energy by convection and the effect of shear instability at the mixed layer base; that is,

$$w_e\delta(w_e)(T - T_e) = \frac{2mu_*^3}{\alpha g h_1}, \quad \text{(A.1f)}$$

where $u_* = \tau_0/\rho_o$ is known as surface frictional velocity, $m$ is the turbulent mixing factor due to wind stirring, and $\alpha$ is the thermal expansion coefficient of the water. The temperature difference between the mixed layer and the entrained water, $T - T_e$, is assumed to be proportional to the vertical temperature gradient in the thermocline layer:

$$T - T_e = h_e \frac{T - T_r}{h - h_1}, \quad \text{(A.1g)}$$

where $T_r$ is the reference temperature in the model deep inert layer and $h_e$ is the thickness of a thin entrainment layer beneath the mixed layer base.

The total downward heat fluxes at the ocean surface:

$$Q_0 = (1 - A)(1 - 0.622C)S_0 - \alpha_a(T - 293) - \gamma(T - 273). \quad \text{(A.1h)}$$

The first rhs term in (A.1h) represents shortwave radiation flux with surface albedo $A = 0.06$, $C$ the frictional cloud cover, and $S_0$ the downward solar radiation flux reaching sea surface under clear sky. The second rhs term denotes surface latent heat flux with a latent heating coefficient $\alpha_a$ (Wang and Li 1993); the last rhs term represents longwave radiation flux with a coefficient $\gamma = 1.8$ W m$^{-2}$ K$^{-1}$ (Seager et al. 1988).

The prognostic equations (A.1a)–(A.1d) along with the diagnostic equations (A.1e)–(A.1h) consist of a close set of the ocean model governing equations.

### b. Linearization of thermodynamic processes

#### 1) THE WARM POOL REGIME

In the governing equations (A.1), the nonlinearity is associated with mixed layer entrainment process. Assume that the perturbation entrainment rate is smaller than the mean entrainment rate. Linearization of the thermodynamic equation (A.1d) with respect to a thermal equilibrium basic state leads to

$$\frac{\partial T'}{\partial t} = -\frac{1}{H_1}[\overline{w}_e(T' - T'_e) + w'_e(\overline{T} - \overline{T}_e)] + \frac{Q'_0}{\rho_o c_w H_1}, \quad \text{(A.2)}$$

where the overbar and the superscript $'$ denote basic state and perturbation variables, respectively.

Assume that a thermal equilibrium basic state in the warm pool regime can be obtained by considering a balance among the total mean downward heat flux, $\overline{Q}_0$, and the cooling associated with mean turbulent entrainment, $\overline{w}_e$, induced by mean frictional wind speed $\overline{u}_*$. From (A.1d), (A.1f), and (A.1g), one can show that the basic state $\overline{w}_e$ and $\overline{Q}_0$ are related to the mean surface frictional wind speed $\overline{u}_*$ by

$$\overline{w}_e = \frac{2mH_2}{\alpha g H_1(\overline{T} - T_r)h_e}\overline{u}_*^3, \quad \text{(A.3a)}$$

$$\overline{Q}_0 = \frac{2m\rho_o c_w}{\alpha g H_1}\overline{u}_*^3, \quad \text{and} \quad \text{(A.3b)}$$

$$\overline{T} - \overline{T}_e = h_e \frac{\overline{T} - T_r}{H_2}. \quad \text{(A.3c)}$$

It can also be shown that the linear versions of Eqs. (A.1f), (A.1g) take the following forms:

$$w_e' = \overline{w}_e\left[3\frac{U'}{\overline{U}} - \frac{T'}{\overline{T}-T_r} + \frac{h'}{H_2} - \frac{H}{H_2}\frac{h_1'}{H_1}\right] \quad \text{and (A.4a)}$$

$$T' - T_e' = \frac{h_e}{H_2}\left[T' - \frac{\overline{T}-T_r}{H_2}(h' - h_1')\right]. \quad \text{(A.4b)}$$

Assuming that the perturbation cloudiness $C'$ is proportional to the perturbation surface wind convergence with a coefficient, $\lambda$, the perturbation downward surface heat flux can be expressed, from (A.1h), as

$$Q_0' = 0.622(1 - A)S_0\lambda\left(\frac{\partial U'}{\partial x} + \frac{\partial V'}{\partial y}\right) - \alpha_a(\overline{T} - 293)\frac{U'}{\overline{U}} - (\alpha_a + \gamma)T'. \quad \text{(A.4c)}$$

Use of (A.1e) and (A.4a) in (A.1c) leads to the following mixed layer depth equation:

$$\frac{\partial h_1'}{\partial t} = E\overline{U}U' + \overline{w}_e\left(3\frac{U'}{\overline{U}} + \frac{h'}{H_2} - \frac{H}{H_2}\frac{h_1'}{H_1}\right). \quad \text{(A.5)}$$

A small term $T'/(\overline{T} - T_r)$ is neglected in deriving (A.5). Substituting (A.4a)–(A.4c) into (A.2) yields the following mixed layer temperature equation:

$$\frac{\partial T'}{\partial t} = D_{rad}\left(\frac{\partial U'}{\partial x} + \frac{\partial V'}{\partial y}\right) - D_{ent}\left(\frac{3U'}{\overline{U}} - \frac{h_1'}{H_1}\right) - D_{eva}\left(\frac{U'}{\overline{U}} + \frac{T'}{\overline{T} - 293}\right) - \mu_o T', \quad \text{(A.6)}$$

where coefficients

$$D_{rad} = 0.622(1 - A)S_0\lambda/\rho_o c_w H_1, \quad \text{(A.6a)}$$

$$D_{ent} = \overline{w}_e(\overline{T} - \overline{T}_e)/H_1, \quad \text{(A.6b)}$$

$$D_{eva} = \alpha_a(\overline{T} - 293)/\rho_o c_w H_1, \quad \text{and (A.6c)}$$

$$\mu_o = \gamma/\rho_o c_w H_1. \quad \text{(A.6d)}$$

Equations (A.1a), (A.1b), (A.5), and (A.6) are linearized governing equations for the active upper-ocean dynamics and mixed layer physics in the warm pool regime.

### 2) THE COLD TONGUE REGIME

Over the equatorial eastern Pacific prevail mean surface easterlies and upwelling. The corresponding thermocline is shallow. The ocean dynamics have an essential control on SST variation, whereas the entrainment is of secondary importance. If the mixed layer depth can be treated as a constant. $H_1$, from (A1c):

$$w_e = w_{up} = H_1\nabla\cdot\mathbf{v}_1 = -E|\overline{U}|U, \quad \text{(A.7)}$$

where $w_{up}$ is the upwelling velocity generated by Ekman pumping, and $E$ is the Ekman coefficient defined by (A.1e′). The perturbation upwelling $w_{up}' = -E|\overline{U}|U'$. Replacing $w_e$ by $w_{up}$ and applying (A.3c), (A.4b), and (A.4c) in (A.2) yields the following mixed-layer temperature equation in the cold tongue:

$$\frac{\partial T'}{\partial t} = D_{up}\frac{h'}{H_2} + D_{rad}\left(\frac{\partial U}{\partial x} + \frac{\partial V}{\partial y}\right) - (D_{up} + D_{eva})\frac{U}{\overline{U}} - \tilde{\mu}_o T', \quad \text{(A.8)}$$

where the coefficients

$$D_{up} = -E|\overline{U}|\overline{U}(\overline{T} - \overline{T}_e)/H_1, \quad \text{(A.8a)}$$

$$\tilde{\mu}_o = D_{up}/(\overline{T} - T_r) + D_{eva}/(\overline{T} - 293) + \gamma/\rho_o c_w H_1. \quad \text{(A.8b)}$$

Equations (A.1a), (A.1b), and (A.8) are linearized governing equations for the active upper-ocean dynamics and mixed layer physics in the cold tongue regime.

## REFERENCES


Battisti, D. S., and A. C. Hirst, 1989: Interannual variability in a tropical atmosphere–ocean model: Influence of the basic state, ocean geometry and nonlinearity. *J. Atmos. Sci.,* **46,** 1687–1712.

Cane, M. A., 1979: The response of an equatorial ocean to simple wind stress pattern. Part I: Model formulation and analytical results. *J. Mar. Res.,* **37,** 233–252.

——, and S. E. Zebiak, 1985: A theory for El Niño and Southern Oscillation. *Science,* **228,** 1084–1087.

Chen, S. S., R. A. Houze Jr., and B. E. Mapes, 1996: Multiscale variability of deep convection in relation to large-scale circulation during TOGA COARE. *J. Atmos. Sci.,* **53,** 1380–1409.

Chen, T. C., and M. Murakami, 1988: The 30–50 day variation of convective activity over the western Pacific Ocean with the emphasis on the northwestern region. *Mon. Wea. Rev.,* **116,** 892–906.

Chou, S.-H., C.-L. Shie, R. M. Atlas, and J. Ardizzone, 1995: The December 1992 westerly wind burst and its impact on evaporation determined from SSMI data. *Proc. Int. Scientific Conf. on the Tropical Ocean Global Atmosphere Program,* Melbourne, Australia, World Meteor. Org., 489–493.

Davey, M. K., and A. E. Gill, 1987: Experiments on tropical circulation with a simple moist model. *Quart. J. Roy. Meteor. Soc.,* **113,** 1237–1269.

Davies, H. C., 1979: Phase-lagged wave CISK. *Quart. J. Roy. Meteor. Soc.,* **105,** 325–353.

Fasullo, J., and P. Webster, 1995: Aspects of ocean/atmosphere interaction during westerly wind bursts. *Proc. Int. Scientific Conf. on the Tropical Ocean Global Atmosphere Program,* Melbourne, Australia, World Meteor. Org., 39–43.

Gill, A. E., 1980: Some simple solutions for heat-induced tropical circulation. *Quart. J. Roy. Meteor. Soc.,* **106,** 447–462.

Godfrey, S. P., and Coauthors, 1995: Surface fluxes and mixed layer heat and freshwater budgets in TOGA-COARE. *Proc. Int. Scientific Conf. on the Tropical Ocean Global Atmosphere Program,* Melbourne, Australia, World Meteor. Org., 464–468.

Hendon, H. H., and M. L. Salby, 1994: The life cycle of the Madden–Julian Oscillation. *J. Atmos. Sci.,* **51,** 2225–2237.

Hirst, A. C., 1986: Unstable and damped equatorial modes in simple coupled ocean–atmosphere models. *J. Atmos. Sci.,* **43,** 606–630.

——, and K.-M. Lau, 1990: Intraseasonal and interannual oscillations in coupled ocean–atmosphere models. *J. Climate,* **3,** 713–725.

Johnson, R. H., 1995: Variability of clouds and precipitation during TOGA COARE. *Proc. Int. Scientific Conf. on the Tropical Ocean Global Atmosphere Program,* Melbourne, Australia, World Meteor. Org., 552–556.

Jones, C., and B. C. Weare, 1996: The role of low-level moisture convergence and ocean latent heat fluxes in the Madden and Julian oscillation: An observational analysis using ISCCP data and ECMWF analyses. *J. Climate,* **9,** 3086–3104.

Kawamura, R., 1988: Intraseasonal variability of sea surface temperature over the tropical western Pacific. *J. Meteor. Soc. Japan,* **66,** 1007–1012.

Krishnamurti, T. N., D. K. Dosterhof, and A. V. Mehta, 1988: Air–sea interaction on the time scale of 30 to 50 days. *J. Atmos. Sci.,* **45,** 1304–1322.

Lau, K.-M., and S. Shen, 1988: On the dynamics of intraseasonal oscillations and ENSO. *J. Atmos. Sci.,* **45,** 1781–1797.

——, and C. H. Sui, 1997: Mechanisms of short-term sea surface temperature regulation: Observations during TOGA COARE. *J. Climate,* **10,** 465–472.

Lin, X., and R. H. Johnson, 1996: Kinematic and thermodynamic characteristics of the flow over the western Pacific warm pool during TOGA COARE. *J. Atmos. Sci.,* **53,** 695–715.

Lindzen, R. S., and S. Nigam, 1987: On the role of the sea surface temperature gradients in forcing low-level winds and convergence in the Tropics. *J. Atmos. Sci.,* **44,** 2440–2458.

Madden, R. A., and P. R. Julian, 1971: Detection of a 40–50 day oscillation in the zonal wind in the tropical Pacific. *J. Atmos. Sci.,* **28,** 702–708.

Miyahara, S., 1987: A simple model of the tropical intraseasonal oscillation. *J. Meteor. Soc. Japan,* **65,** 341–351.

Murakami, T., 1980: Empirical orthogonal function analysis of satellite observed outgoing longwave radiation during summer. *Mon. Wea. Rev.,* **108,** 205–222.

Nakazawa, T., 1995: Intraseasonal oscillations during the TOGA COARE IOP. *J. Meteor. Soc. Japan,* **73,** 305–319.

Neelin, J. D., 1989: On the interpretation of the Gill model. *J. Atmos. Sci.,* **46,** 2466–2468.

——, 1991: The slow sea surface temperature mode and the fast-wave limit: Analytic theory for tropical interannual oscillations and experiments in a hybrid coupled model. *J. Atmos. Sci.,* **48,** 584–606.

Niiler, P. P., and E. B. Kraus, 1977: One-dimensional models of upper ocean. *Modeling and Prediction of the Upper Layers of the Ocean,* E. B. Kraus, Ed., Pergamon Press, 143–172.

Nitta, T., 1987: Convective activities in the tropical western Pacific and their impact on the Northern Hemisphere summer monsoon. *J. Meteor. Soc. Japan,* **65,** 373–390.

Philander, S. G. H., T. Yamagata, and R. C. Pacanowski, 1984: Unstable air–sea interactions in the tropics. *J. Atmos. Sci.,* **41,** 604–613.

Rui, H., and B. Wang, 1990: Development characteristics and dynamic structure of tropical intraseasonal convective anomalies. *J. Atmos. Sci.,* **47,** 357–379.

Salby, M. L., and H. H. Hendon, 1994: Intraseasonal behavior of clouds, temperature, and motion in the Tropics. *J. Atmos. Sci.,* **51,** 2207–2224.

Seager, R., S. E. Zebiak, and M. A. Cane, 1988: A model of tropical Pacific sea surface temperature climatology. *J. Geophys. Res.,* **93** (C2), 1265–1280.

Suarez, M. J., and P. S. Schopf, 1988: A delayed action oscillator for ENSO. *J. Atmos. Sci.,* **45,** 3283–3287.

Sui, C.-H., X. Li, K.-M. Lau, and D. Adamac, 1997: Multiscale air–sea interactions during TOGA COARE. *Mon. Wea. Rev.,* **125,** 448–462.

Wang, B., 1988a: Dynamics of tropical low-frequency waves: An analysis of the moist Kelvin wave. *J. Atmos. Sci.,* **45,** 2051–2065.

——, 1988b: Comments on ''An air–sea interaction model of intraseasonal oscillation in the tropics.'' *J. Atmos. Sci.,* **45,** 3521–3525.

——, and H. Rui, 1990: Synoptic climatology of transient tropical intraseasonal convective anomalies: 1975–1985. *Meteor. Atmos. Phys.,* **44,** 43–61.

——, and T. Li, 1993: A simple tropical atmospheric model of relevance to short-term climate variation. *J. Atmos. Sci.,* **50,** 260–284.

——, and Z. Fang, 1996: Chaotic oscillations of tropical climate: A dynamic system theory for ENSO. *J. Atmos. Sci.,* **53,** 2786–2802.

——, and X. Xie, 1997: A model for the boreal summer intraseasonal oscillation. *J. Atmos. Sci.,* **54,** 72–86.

——, ——, and P. Chang, 1995: An intermediate model of the tropical Pacific Ocean. *J. Phys. Oceanogr.,* **25,** 1599–1616.

Yamagata, T., 1985: Stability of a simple air–sea coupled model in the Tropics. *Coupled Ocean–Atmosphere Models,* J. C. J. Nihoul, Ed., Elsevier Oceanography Series, No. 40, Elsevier, 637–657.

Zebiak, S. E., 1986: Atmospheric convergence feedback in a simple model for El Niño. *Mon. Wea. Rev.,* **114,** 1263–1271.

——, and M. A. Cane, 1987: A model ENSO. *Mon. Wea. Rev.,* **115,** 2262–2278.

Zhang, C., 1996: Atmospheric intraseasonal variability at the surface in the tropical western Pacific Ocean. *J. Atmos. Sci.,* **53,** 739–758.